A Novel Neutralizing Antibody Targeting Receptor Binding Domain of SARS-CoV-2

Soo-Young Lee (SOOYOUNG.LEE@CELLTRION.COM)
Celltrion Inc. https://orcid.org/0000-0002-3306-9333

Cheolmin Kim
Celltrion Inc.

Dong-Kyun Ryu
Celltrion Inc. https://orcid.org/0000-0003-4237-4740

Jihun Lee
Celltrion Inc. https://orcid.org/0000-0002-8803-7689

Young-Il Kim
Chungbuk National University

Ji-Min Seo
Celltrio Inc.

Yeon-Gil kim
Pohang University of Science and Technology

Jae-Hee Jeong
Pohang University of Science and Technology

Minsoo Kim
Celltrion Inc.

Jong-In Kim
Celltrion Inc.

Pankyeom Kim
Celltrion Inc.

Jin Soo Bae
Celltrion Inc. https://orcid.org/0000-0001-7484-9048

Eun Yeong Shim
Celltrion Inc.

Min Seob Lee
Celltrion Inc.

Man Su Kim
Celltrion Inc.

Hanmi Noh
Celltrion Inc.

Geun-Soo Park

Celltrion Inc.
Jae Sang Park
Celltrion Inc.
Dain Son
Celltrion Inc.
Yongjin An
Celltrion Inc.
Jeong No Lee
Celltrion Inc.
Ki-Sung Kwon
Celltrion Inc.
Joo-Yeon Lee
Korea Centers for Disease Control and Prevention
Hansaem Lee
Korea Centers for Disease Control and Prevention
Jeong-Sun Yang
Korea Centers for Disease Control and Prevention
Kyung-Chang Kim
Korea Centers for Disease Control and Prevention
Sung Soon Kim
Korea Centers for Disease Control and Prevention
Hye-Min Woo
Korea Centers for Disease Control and Prevention
Jun-Won Kim
Korea Centers for Disease Control and Prevention
Man-Seong Park
Department of Microbiology, College of Medicine, Hallym University, Chuncheon, Gangwon-do, Republic of Korea
Kwang-Min Yu
Chungbuk National University
Se-Mi Kim
Chungbuk National University
Eun-Ha Kim
Chungbuk National University
Su-Jin Park
Chungbuk National University
Seong Tae Jeong
Agency for Defense Development
Chi Ho Yu

Agency for Defense Development
Youngjo Song
Agency for Defense Development
Se Hun Gu
Agency for Defense Development
Hanseul Oh
Korea Research Institute of Bioscience and Biotechnology
Bon-Sang Koo
Korea Research Institute of Bioscience and Biotechnology
Jung Joo Hong
Korea Research Institute of Bioscience and Biotechnology
Choong-Min Ryu
Korea Research Institute of Biosciences and Biotechnology
Wan Beom Park
Seoul National University College of Medicine
Myoung-don Oh
Seoul National University College of Medicine
Young Ki Choi
Chungbuk National University https://orcid.org/0000-0002-0872-0147

Article

Keywords:

Posted Date: September 10th, 2020

DOI: https://doi.org/10.21203/rs.3.rs-59639/v1

Version of Record: A version of this preprint was published at Nature Communications on January 12th, 2021. See the published version at https://doi.org/10.1038/s41467-020-20602-5.

Abstract

Severe acute respiratory syndrome coronavirus 2 (SARS-CoV-2) has caused the current COVID-19 global pandemic. Vaccines and therapeutics are urgently needed for this highly transmissible virus. In this study, we screened human monoclonal antibodies (mAbs) targeting the receptor binding domain (RBD) of the SARS-CoV-2 spike protein from an antibody library constructed from peripheral blood mononuclear cells of a COVID-19 convalescent patient. A potent neutralizing antibody, termed CT-P59, was identified and found to be effective against various SARS-CoV-2 isolates including the D614G spike protein variant without antibody-dependent enhancement effect. Complex crystal structure of CT-P59 Fab/SARS-CoV-2 RBD showed that CT-P59 blocks interaction regions of SARS-CoV-2 RBD for its cellular receptor, angiotensin converting enzyme 2 (ACE2). The binding orientation of CT-P59 is notably different from the previously reported neutralizing mAbs targeting SARS-CoV-2 RBD suggesting that CT-P59 can be a novel binder to SARS-CoV-2 RBD. Therapeutic effects of CT-P59 were evaluated in three animal models (ferret, hamster, and rhesus monkey), and a substantial reduction in viral titre along with alleviation of clinical symptoms was observed. These findings suggest that the human monoclonal antibody, CT-P59, is a promising therapeutic candidate for treatment of COVID-19.

Main Text

Screening and characterization of CT-P59

To identify novel SARS-CoV-2 targeting neutralizing antibodies, we isolated RBD-binding single-chain variable fragments by utilizing recombinant SARS-CoV-2 RBD as a bait for phage display screening. A monoclonal antibody reformatted to a fully human immunoglobulin (IgG), termed CT-P59, was assessed for its neutralization potency by *in vitro* plaque reduction neutralization test (PRNT) against authentic SARS-CoV-2 and SARS-CoV-2 D614G variant. CT-P59 was shown to significantly inhibit viral replication with the value of low half-maximal inhibitory concentration (IC_{50}) (8.37 ng/ml) against a SARS-CoV-2 clinical isolate in Korea, which showed identical genome sequence of S protein with the primary virus in China (Accession ID: YP_009724390.1). Intriguingly, we found that CT-P59 more effectively reduced the replication of D614G variant with the value of IC_{50} (5.73 ng/ml) than that of the wild virus having D614 amino acid in S protein (Fig. 1a). In addition, a competitive binding assay with biolayer interferometry (BLI) revealed that CT-P59 completely inhibited the binding of RBD-ACE2 (Fig. 1b). In parallel, we carried out the RBD binding and ACE2 interference test with RBD mutant proteins which were reported and commercially available[9,12,13]. We found that CT-P59 can bind to these mutants and completely inhibit binding between ACE2 and RBD mutants (Extended Data Table 1 and Fig. 1b). Next, surface plasmon resonance analysis demonstrated that CT-P59 has high affinity for SARS-CoV-2 RBD with a K_D value of 27 pM (Extended Data Fig. 1). Furthermore, CT-P59 binding specificity to other coronaviruses (SARS, HCoV-HKU1, and MERS) was evaluated by BLI, indicating that CT-P59 can bind specifically to SARS-CoV-2. (Extended Data Fig. 2).

Structural basis of neutralization

To investigate the neutralizing mechanism of CT-P59, the crystal structure of the CT-P59 Fab/SARS-CoV-2 RBD complex was determined using X-ray crystallography at 2.7 Å resolution (Extended Data Table 2). The complex structure shows that CT-P59 binds to the receptor binding motif (RBM) within SARS-CoV-2 RBD, which directly interacts with ACE2 (Fig. 2a). The association angle between CT-P59 and the RBD is different from that reported for other neutralizing antibodies in complex with the RBD (Fig. 2b) [14,15]. These observations indicate that the epitope of CT-P59 are unique from those of other antibodies[14-19] (Fig. 2c). Further, the interactions of the RBD with the heavy and light chains of CT-P59 bury a solvent-accessible surface area of 824.6 and 112.5 $Å^2$, respectively. Consistently, most of the interaction between the two proteins is mediated by the heavy chain involving all three complementarity determining regions (CDRs). In total, 16 residues from the CT-P59 heavy chain interact with 19 residues of the RBD at a distance cut-off of 4.5 Å (Extended Data Table 3). Of note, the β-hairpin structure of the CDR H3 plays a crucial role in the strong association with the RBD, by forming eight hydrogen bonds as well as hydrophobic interactions involving several of aromatic residues in the middle of the ACE2 binding surface (Fig. 2d). The light chain shows marginal contact with the RBD involving parts of CDR L1 and L2 where only three residues interact with four residues of the RBD (Extended Data Table 3).

To further analyse the structural basis for blocking of the interaction between RBD and ACE2 by CT-P59, the complex structure of CT-P59-RBD was superimposed on the RBD-ACE2 structure (PDB 6LZG)[20]. CT-P59 binding does not alter the overall conformation of the RBD structure in which the pairwise root mean square deviation between the Cα atoms of the two RBD structures is 0.89 Å over 193 atoms. However, the β5–β6 loop region (residues 473–488) of the RBD shows a local conformational change, which might be induced by the interaction with CT-P59. The structural superposition reveals that the heavy chain of CT-P59 overlaps completely with ACE2 protein, while the light chain overlaps partially with the receptor (Extended Data Fig. 3a). In agreement with the superposition, there is substantial overlap between the CT-P59 and ACE2 binding surface areas on RBD (Extended Data Fig. 3b). Among the 21 residues of RBD that interact with ACE2, 12 are also involved in the interaction with CT-P59, when a distance cut-off of 4.5 Å is applied (Fig. 2c). These observations indicate that the binding of CT-P59 to RBD directly occludes the binding surface of ACE2.

In vivo efficacy in animal models

To demonstrate *in vivo* antiviral efficacy of CT-P59 in terms of viral clearance and clinical symptoms, viral loads and lung pathology, we conducted virus challenge studies employing three animal models (ferrets, golden Syrian hamsters, and rhesus monkeys). In the ferret study, viruses were challenged via both intranasal and intratracheal routes, followed by intravenous treatment of CT-P59 and isotype control at 1 day post-infection (dpi). At 2 dpi, the infectious virus titre ($TCID_{50}$) in nasal wash was significantly decreased when compared to controls in time- and dose-dependent manners, and the infectious virus was not detected at 6 dpi in animals treated with 30 mg/kg of CT-P59. For rectal swabs, the viral RNA copies were significantly decreased from 4 dpi at both doses (Fig. 3a and 3b). Further, the infectious virus titre

was significantly attenuated in lung tissues with both doses at 3 dpi and not detectable with 30 mg/kg at 7 dpi (Extended Data Fig. 6a). The reduction of viral load in the upper and lower respiratory tract was consistent with an improvement in clinical symptoms and lung pathology (Supplementary Table 1 and Extended Data Fig. 7). To compare the therapeutic effect of CT-P59 with a World Health Organization (WHO) approved drug, Remdesivir was administered daily for 5 days (18 mg/kg) in ferrets following 1 day of SARS-CoV-2 infection. Remdesivir-treated ferrets showed attenuated virus titres and viral RNAs in respiratory tracts and rectal swabs respectively, compared with those of isotype control-treated animals, but the infectious virus was detected in the respiratory tract until 6 dpi (Fig. 3a, b) suggesting delayed clearance of SARS-CoV-2 in ferrets compared with the CT-P59-treated group.

In SARS-CoV-2-infected golden Syrian hamsters, the viral load reached peak levels on 3 dpi (8.3 log $TCID_{50}$/g) in the lungs of vehicle-treated hamsters and slightly declined by 5 dpi (6.8 log $TCID_{50}$/g, Extended Data Fig. 6b). In CT-P59-treated hamsters, there was significant attenuation of viral loads in lungs in the 15 mg/kg treated group, and all other groups (range, 30-90 mg/kg) showed no infectious virus in lung tissues 48 hours after CT-P59 treatment, suggesting complete inhibition of SARS-CoV-2 replication in lungs of golden Syrian hamster from 30 mg/kg dose (Extended Data Fig. 6b).

In the rhesus monkey study, no apparent clinical manifestations including fever, weight loss, and respiratory distress, were observed in both CT-P59- and vehicle control-treated animals. The viral load reached peak levels on 2 dpi (4.3 log $TCID_{50}$/ml) in nasal swabs, and then gradually declined until 6 dpi in vehicle-treated control group (Fig. 3c). In contrast, CT-P59 treatment rapidly reduced virus titres and the infectious virus was not detected even at 2 dpi following the CT-P59 administration in both 45 and 90 mg/kg groups. Further no viral RNAs were detected in rectal swabs collected from CT-P59-treated animals from 4 dpi (Fig. 3d). All monkeys were euthanized at 6 dpi and individual lung lobes were collected to quantify the infectious virus titre. No infectious virus was detected in any of the lung lobes tested from any animals, including vehicle control- and CT-P59-treated groups (Extended Data Fig. 6c).

To further investigate possible adverse effect, we performed the *in vitro* ADE assay with authentic SARS-CoV-2. No increase in the viral infections was observed in Fc receptor-bearing cells (Extended Data Fig. 5).

Discussion

In this study, we demonstrated the potential therapeutic benefit of neutralizing antibody CT-P59 targeting RBD of SARS-CoV-2 in *in vitro* and *in vivo* studies. We found that CT-P59 binds to RBD of S protein, rendering complete steric hindrance interfering with the viral binding to ACE2 by BLI competition assay and X-ray crystallography. Importantly, CT-P59 significantly inhibited the viral replication of clinical isolates by *in vitro* PRNT. Unlike RBD-targeting antibodies with similar sensitivities to the viral neutralization on a D614G variant[21], CT-P59 can effectively neutralize D614G variant; the underlying mechanism remains to be elucidated in terms of S protein stability and viral kinetics.

SARS-CoV-2 RBD mutations might alter the binding affinity of the virus for ACE2[9,12,13]. For instance, V367F, W436R, and D364Y were reported to increase the binding affinity for ACE2, which might accelerate viral spread further perpetuating the pandemic. We found that CT-P59 binds to RBD mutant proteins and also interferes with ACE2 (Extended Data Table 1 and Fig. 1b). In addition, according to the X-ray crystallography data (Fig. 2 and Extended Data Fig. 3), CT-P59 does not bind to the amino acid residues at position 367, 436, or 364 of the RBD. These results suggest that CT-P59 might be able to neutralize naturally occurring potential variants.

The complex structure of CT-P59 shows that CT-P59 inhibits SARS-CoV-2 RBD binding to its cellular receptor, ACE2, by blocking substantial areas of the ACE2 interaction regions. Among the previously reported neutralizing antibodies against SARS-CoV-2 RBD that specifically block ACE2 binding, we compared the publicly available atomic coordinates with those of CT-P59 to evaluate association mode between antibodies and RBD (Extended Data Fig. 4a). We found that the majority of the ACE2 blocking antibodies—including CB6[16], B38[17], CV30[18], CC 12.1[19], CC 12.3[19] and REGN10933[14]—adopt a similar orientation when bound to RBD. Each of these antibodies belong to the immunoglobulin heavy chain variable region genes (IGHV) 3 germline that is the most frequently used IGHV gene among the known SARS-CoV-2 neutralizing antibodies[22]. The neutralizing antibody P2B-2F6[15] which is based on the IGHV4-38 gene, on the other hand, interacts with RBD at about a 90 degree angle from the previous group. Notably, CT-P59 (based on IGHV2-70) binds with an orientation in the middle of these mAb groups (Extended Data Fig. 4a) and shares portions of the epitope from each group (Fig. 2c). To our knowledge, CT-P59 is the first SARS-CoV-2 RBD neutralizing antibody with an IGHV2 germline lineage that its high resolution structure reported. Cryo-electron microscopy has revealed that RBD of SARS-CoV-2 S protein trimer undergoes either “up” or “down” conformations and ACE2 can only bind to the “up” conformation[23,24]. Structural alignment of each group of neutralizing antibodies with the “down” form of SARS-CoV-2 S protein trimers showed that the IGHV3 antibody group heavily clashes with the adjacent RBD protomer, whereas P2B-2F6 can bind to the trimer without any collision with the adjacent molecules (Extended Data Fig. 4b). Although CT-P59 collides with the Asn343 glycosylated site on adjacent protomer, it has much fewer clashes compared with IGHV3 group antibodies. All the evaluated antibodies can interact with RBD on the “up” conformation without any steric hindrance. We therefore propose that CT-P59 may have more chance to block ACE2-RBD interaction in pre-fusion state than IGHV3 group antibodies if there is slight hinge-like movement in RBD region.

Because no animal models are available that accurately reflect clinical symptoms (e.g. lung damage) of patients with severe COVID-19[25-29], ferrets, Syrian hamsters and rhesus monkeys have been used together for evaluation of SARS-COV-2 pathogenesis/transmission and to assess the efficacy of therapeutics and vaccines against COVID-19[30-33]. *In vivo* challenge studies using these models has demonstrated that CT-P59 is capable of quickly decreasing virus titres, particularly improving clinical symptoms and pathological changes in ferrets. Notably, when we compared the therapeutic efficacy of CT-P59 with Remdesivir, a **drug for use in hospitalized patients with COVID-19**, the CT-P59-treated ferrets

showed more attenuated viral loads in upper respiratory tracts from 2 dpi. The early clearance of infectious virus suggests that CT-P59 might be an option for COVID-19 patients as combination therapy.

Concerning ADE[34,35], the *in vitro* assay indicated no CT-P59-mediated increase in authentic viral infections in FcR-bearing cells and permissive cells (Extended Data Fig. 5), in line with no worsening of symptoms in CT-P59-treated animals as described above. Moreover, a recent animal study showed that ADE was not observed by vaccine targeting SARS-CoV-2 RBD[11]. Therefore, these observations suggest that CT-P59 can remarkably neutralize SARS-CoV-2 via binding to RBD and ameliorate pathological symptoms without ADE during clinical trials.

References

1 Shen, C. *et al.* Treatment of 5 Critically Ill Patients With COVID-19 With Convalescent Plasma. *JAMA*, doi:10.1001/jama.2020.4783 (2020).

2 Li, L. *et al.* Effect of Convalescent Plasma Therapy on Time to Clinical Improvement in Patients With Severe and Life-threatening COVID-19: A Randomized Clinical Trial. *JAMA*, doi:10.1001/jama.2020.10044 (2020).

3 Salazar, E. *et al.* Treatment of Coronavirus Disease 2019 (COVID-19) Patients with Convalescent Plasma. *Am J Pathol* **190**, 1680-1690, doi:10.1016/j.ajpath.2020.05.014 (2020).

4 Li, F., Li, W., Farzan, M. & Harrison, S. C. Structure of SARS coronavirus spike receptor-binding domain complexed with receptor. *Science* **309**, 1864-1868, doi:10.1126/science.1116480 (2005).

5 Li, F. Structure, Function, and Evolution of Coronavirus Spike Proteins. *Annu Rev Virol* **3**, 237-261, doi:10.1146/annurev-virology-110615-042301 (2016).

6 Shang, J. *et al.* Structural basis of receptor recognition by SARS-CoV-2. *Nature* **581**, 221-224, doi:10.1038/s41586-020-2179-y (2020).

7 Tai, W. *et al.* Characterization of the receptor-binding domain (RBD) of 2019 novel coronavirus: implication for development of RBD protein as a viral attachment inhibitor and vaccine. *Cell Mol Immunol* **17**, 613-620, doi:10.1038/s41423-020-0400-4 (2020).

8 Zhang, L. *et al.* The D614G mutation in the SARS-CoV-2 spike protein reduces S1 shedding and increases infectivity. *bioRxiv*, doi:10.1101/2020.06.12.148726 (2020).

9 Korber, B. *et al.* Spike mutation pipeline reveals the emergence of a more transmissible form of SARS-CoV-2. *bioRxiv* (2020).

10 Li, Q. *et al.* The Impact of Mutations in SARS-CoV-2 Spike on Viral Infectivity and Antigenicity. *Cell*, doi:10.1016/j.cell.2020.07.012 (2020).

11 Quinlan, B. D. *et al.* The SARS-CoV-2 receptor-binding domain elicits a potent neutralizing response without antibody-dependent enhancement. *bioRxiv*, doi:https://doi.org/10.1101/2020.04.10.036418 (2020).

12 Ou, J. *et al.* Emergence of RBD mutations in circulating SARS-CoV-2 strains enhancing the structural stability and human ACE2 receptor affinity of the spike protein. *bioRxiv*, doi:https://doi.org/10.1101/2020.03.15.991844 (2020).

13 Nelson-Sathi, S. *et al.* Structural and Functional Implications of Non-synonymous Mutations in the Spike protein of 2,954 SARS-CoV-2 Genomes. *bioRxiv*, doi:https://doi.org/10.1101/2020.05.02.071811 (2020).

14 Hansen, J. *et al.* Studies in humanized mice and convalescent humans yield a SARS-CoV-2 antibody cocktail. *Science*, doi:10.1126/science.abd0827 (2020).

15 Ju, B. *et al.* Human neutralizing antibodies elicited by SARS-CoV-2 infection. *Nature*, doi:10.1038/s41586-020-2380-z (2020).

16 Shi, R. *et al.* A human neutralizing antibody targets the receptor-binding site of SARS-CoV-2. *Nature*, doi:10.1038/s41586-020-2381-y (2020).

17 Wu, Y. *et al.* A noncompeting pair of human neutralizing antibodies block COVID-19 virus binding to its receptor ACE2. *Science* **368**, 1274-1278, doi:10.1126/science.abc2241 (2020).

18 Hurlburt, N. K. *et al.* Structural basis for potent neutralization of SARS-CoV-2 and role of antibody affinity maturation. *bioRxiv*, doi:https://doi.org/10.1101/2020.06.12.148692 (2020).

19 Yuan, M. *et al.* Structural basis of a public antibody response to SARS-CoV-2. *bioRxiv*, doi:10.1101/2020.06.08.141267 (2020).

20 Wang, Q. *et al.* Structural and Functional Basis of SARS-CoV-2 Entry by Using Human ACE2. *Cell* **181**, 894-904 e899, doi:10.1016/j.cell.2020.03.045 (2020).

21 Yurkovetskiy, L. *et al.* SARS-CoV-2 Spike protein variant D614G increases infectivity and retains sensitivity to antibodies that target the receptor binding domain. *bioRxiv*, doi:10.1101/2020.07.04.187757 (2020).

22 Yuan, M. *et al.* Structural basis of a shared antibody response to SARS-CoV-2. *Science*, doi:10.1126/science.abd2321 (2020).

23 Wrapp, D. *et al.* Cryo-EM structure of the 2019-nCoV spike in the prefusion conformation. *Science* **367**, 1260-1263, doi:10.1126/science.abb2507 (2020).

24 Walls, A. C. *et al.* Structure, Function, and Antigenicity of the SARS-CoV-2 Spike Glycoprotein. *Cell* **181**, 281-292 e286, doi:10.1016/j.cell.2020.02.058 (2020).

25 Cleary, S. J. *et al.* Animal models of mechanisms of SARS-CoV-2 infection and COVID-19 pathology. *Br J Pharmacol*, doi:10.1111/bph.15143 (2020).

26 Bao, L. *et al.* The pathogenicity of SARS-CoV-2 in hACE2 transgenic mice. *Nature*, doi:10.1038/s41586-020-2312-y (2020).

27 Chan, J. F. *et al.* Simulation of the clinical and pathological manifestations of Coronavirus Disease 2019 (COVID-19) in golden Syrian hamster model: implications for disease pathogenesis and transmissibility. *Clin Infect Dis*, doi:10.1093/cid/ciaa325 (2020).

28 Williamson, B. N. *et al.* Reinfection could not occur in SARS-2 CoV-2 infected rhesus macaques. *bioRxiv*, doi:https://doi.org/10.1101/2020.04.15.043166 (2020).

29 Deng, W. *et al.* Rhesus macaques can be effectively infected with SARS-CoV-2 via ocular conjunctival route. *bioRxiv*, doi:https://doi.org/10.1101/2020.03.13.990036 (2020).

30 Kim, Y. I. *et al.* Infection and Rapid Transmission of SARS-CoV-2 in Ferrets. *Cell Host Microbe* **27**, 704-709 e702, doi:10.1016/j.chom.2020.03.023 (2020).

31 Sia, S. F. *et al.* Pathogenesis and transmission of SARS-CoV-2 in golden hamsters. *Nature* **583**, 834-838, doi:10.1038/s41586-020-2342-5 (2020).

32 Munster, V. J. *et al.* Respiratory disease in rhesus macaques inoculated with SARS-CoV-2. *Nature*, doi:10.1038/s41586-020-2324-7 (2020).

33 Park, S. J. *et al.* Antiviral Efficacies of FDA-Approved Drugs against SARS-CoV-2 Infection in Ferrets. *mBio* **11**, doi:10.1128/mBio.01114-20 (2020).

34 Jaume, M. *et al.* Anti-severe acute respiratory syndrome coronavirus spike antibodies trigger infection of human immune cells via a pH- and cysteine protease-independent FcgammaR pathway. *J Virol* **85**, 10582-10597, doi:10.1128/JVI.00671-11 (2011).

35 Wang, Q. *et al.* Immunodominant SARS Coronavirus Epitopes in Humans Elicited both Enhancing and Neutralizing Effects on Infection in Non-human Primates. *ACS Infect Dis* **2**, 361-376, doi:10.1021/acsinfecdis.6b00006 (2016).

Methods

Cells and viruses

VeroE6 cells (ATCC, CRL-1586) were cultured in Dulbecco's modified Eagle's medium (DMEM) supplemented with 5% (v/v) fetal bovine serum (FBS) and penicillin-streptomycin (100 U/mL). The SARS-CoV-2 viruses used for *in vitro* PRNT assay[36] were propagated in VeroE6 cells with DMEM supplemented with 2% FBS by BetaCoV/Korea/KCDC03/2020 (Accession ID: EPI_ISL_407193) and hCoV-19/South Korea/KUMC17/2020 (provided by microbiology lab in Korea university), both strains were isolated from Korean COVID-19 patients. The SARS-CoV-2 virus (NMC-nCoV02, isolated from a Korean COVID-19 patient) used for $TCID_{50}$ and ferret challenges was propagated in Vero cells (ATCC, CCL-81). Raji cells (ATCC, CCL-86) and U937 cells (ATCC, CRL-1593.2) were cultured with RPMI-1640 containing 10% FBS and PenStrep (Gibco). Authentic virus infection and animal challenge were conducted in biosafety level-3

Isolation of PBMCs from COVID-19 patient

Blood was collected from a convalescent COVID-19 patient in Korea (IRB 2002-105-110). Samples were obtained 48 h after the disappearance of symptoms, and two consecutive respiratory specimens at an interval of 24 h were confirmed as negative for SARS-CoV-2 by PCR before blood sampling. Peripheral blood mononuclear cells (PBMCs) were isolated from the collected blood using Ficoll-Paque (GE Healthcare), and mRNA was extracted using the TRIzol reagent (Thermo Fisher). The isolated mRNA was immediately converted to cDNA using SuperScript^{TM} III Reverse Transcriptase (Invitrogen).

Phage library construction and biopanning

Antibody variable regions (V_L and V_H) were amplified by PCR with appropriate primers for phage display. ScFvs were generated by linking V_L and V_H fragments and directly cloned into phagemid vector, pComb3xSS, for library construction. ER2738 cells (Lucigen) were transformed with the scFv library, then cultured in SB medium containing 50 μg/mL carbenicillin and VCSM13 helper phage (Stratagene) at 37°C overnight. Next day, phages displaying scFv were harvested for biopanning to screen SARS-CoV-2 RBD-binding scFv displayed on phage. Briefly, SARS-CoV-2 RBD (Sino biological) was coated on magnetic beads (Invitrogen) and incubated with the phage library. Following incubation and washing, SARS-CoV-2 RBD-bound phages were eluted and used to infect fresh ER2738 cells. After several rounds of biopanning, scFv phages binding to SARS-CoV-2 RBD were identified by phage ELISA for further selection.

Preparation of scFv-Fc, full-length IgG and S proteins

Each scFv identified by phage ELISA was cloned into the Fc fusion vector and transiently expressed in Chinese Hamster Ovary (CHO) cells. Next, for the expression of full-length IgG, synthesized DNAs of heavy chain and light chain for each mAb were inserted into MarEx vectors (Celltrion) by enzymatic digestion with *Nhe*I (NEB) / *Pme*I (NEB) and *Hpa*I (NEB) / *Cla*I (NEB), respectively. CR3022 antibody was reconstituted with variable sequences for light and heavy chain according to the published sequence information (US2008/0014204A1). Thereafter, transient expression by co-transfection was performed in

CHO cells. Each scFv-Fc and full-length IgG was purified with affinity chromatography on Protein A (GE Healthcare). For the production of SARS-CoV-2 RBD, DNA encoding the SARS-CoV-2 S protein RBD (YP_009724390.1: Arg319-Asn536) with a polyhistidine tag at the C-terminus was cloned into the MarEx vector and transiently expressed in CHO cells. SARS-CoV-2 RBD with polyhistidine tag was affinity purified using Ni-NTA Resin (Thermo Fisher). Recombinant proteins for RBD and its mutants (A435S, F342L, G476S, K458R, N354D, V367F, V483A, W436R), SARS-CoV S1, HCoV-HKU1 S1 and MERS-CoV RBD were commercial products (Sino Biological).

mAb neutralizing assays

To evaluate the neutralizing activity of monoclonal antibodies, plaque reduction neutralizing tests for SARS-CoV-2 were performed as described previously[37]. Briefly, 2-fold serially diluted mAbs ranging from 10^3 to 1 ng/ml and an equal volume of virus (40 pfu/well) were incubated at 37°C for 2 h. The antibody-virus mixture was inoculated into a 24-well plate seeded with VeroE6 cells (1×10^5 cells/well) and incubated at 37°C for 1 h, followed by overlay of 1 ml of 0.5% agarose (Lonza). After 2 to 3 days of incubation, the cells were fixed with 4% paraformaldehyde and visualized plaques with crystal violet. Two independent experiments were performed in duplicate for each mAb. The data were fitted to a dose-response inhibition model, and the half-maximal inhibitory concentration (IC_{50}) of each mAb was calculated using GraphPad Prism6 software.

Surface plasmon resonance for affinity

Binding affinity of CT-P59 to SARS-CoV-2 RBD was assayed using a Biacore T200^{TM} SPR instrument (Cytiva). SARS-CoV-2 RBD manufactured by Celltrion was covalently immobilized on the CM5 chip using an amine coupling reaction. Any unstable, SARS-CoV-2 RBD was removed by at least six washes of pre-run solution before sample run. CT-P59 was serially diluted from 10 to 0.04 nM using HBS-EP buffer (pH 7.4), and then injected for 120 sec, followed by HBS-EP buffer (pH 7.4) for 120 sec to generate the binding and dissociation curves, respectively. After each cycle, the chip surface was treated with a brief pulse of 20 mM NaOH until the response unit (RU) signal returned to baseline, and then a new cycle was started. The dissociation constant was fitted to a bivalent analyte model using Biacore evaluation software (Cytiva).

Biolayer interferometry (BLI)

Competitive binding to SARS-CoV-2 RBDs between CT-P59 and ACE2, binding specificity and binding affinity to SARS-CoV-2 RBDs were measured by biolayer interferometry (BLI) using the Octet QK^e system (ForteBio). All samples were prepared with corresponding concentration by dilution in Kinetic Buffer (BMS). To determine the competitive characteristics between CT-P59 and ACE2, the immobilized wild type and mutant SARS-CoV-2 RBD proteins with a concentration of 50 nM were saturated with 267 nM of CT-P59 for 5 min, and then flowed with CT-P59 (133.5 nM) in the presence or absence of ACE2 (133.5 nM) for 5 min. As a positive control, buffer was loaded onto SARS-CoV-2 RBD immobilized biosensor, and

flowed ACE2 (133.5 nM). For the binding specificity assay, binding of CT-P59 to four virus S proteins (SARS-CoV-2 RBD, SARS-CoV S1, HCoV-HKU1 S1, MERS RBD) were measured. Each S protein (50 nM) was loaded onto Anti-Penta-HIS Biosensor, and then CT-P59 (267 nM) was flowed for 5 min. Buffer and ACE2 were sequentially flowed for a positive control. To evaluate binding affinity between CT-P59 and SARS-CoV-2 RBD wild type and mutants, CT-P59 (5 nM) was loaded onto Anti-Human IgG Fc Capture Biosensor for 7.5 min, and then each SARS-CoV-2 RBD was flowed with concentration of 0 nM, 2.5 nM, 5 nM, 10 nM and 20 nM for 10 min and 15 min to generate association and dissociation curve, respectively.

Crystallization and structure determination

The CT-P59 Fab/SARS-CoV-2 RBD complex was prepared by mixing the purified SARS-CoV-2 RBD protein with CT-P59 Fab at a 1:1.2 molar ratio. Excess CT-P59 Fab was removed by size exclusion chromatography by using a 16/600 Superdex-200 column (GE Healthcare) equilibrated in 10 mM Tris-HCl (pH 8.0) and 150 mM NaCl. The fractions containing the complex were pooled and concentrated up to 6 mg/ml and used for crystallization experiments. Diffraction quality crystals were obtained at 20°C by the sitting-drop vapor-diffusion method with 0.4 µl protein solution mixed with 0.4 µl of precipitant solution containing 10 mM $NiCl_2$, 0.1 M Tris-HCl (pH 8.0) and 16% (wt/vol) PEG MME 2000. For data collection, the crystals were cryo-protected by briefly soaking in the precipitant containing an additional 20% ethylene glycol and immediately mounted in a stream of gaseous nitrogen at 100 K. X-ray diffraction data were collected at a wavelength of 0.9796 Å using a beamline BL-5C of Pohang Light Source-II, Republic of Korea. The data set was processed using XDS program package[38]. The CT-P59 Fab/SARS-CoV-2 RBD complex structure was determined by molecular replacement using Phaser[39]. The SARS-CoV-2 RBD/CB6 complex structure (PDB code, 7C01) was used as a search model. Model building and refinement were performed using Coot[40] and the Phenix package[41], respectively. The Ramachandran statistics of the final structure are 96.81% in most favored region, 3.19% in allowed region and 0.00% in disallowed region. The X-ray diffraction and structure refinement statistics are summarized in Extended Data Table 2. All structure figures were generated with PyMol[42].

In vitro ADE assay

VeroE6 cells ($1x10^4$/well) were seeded in 96-well plate at 24 h before infection. Next day, antibodies (CT-P59, CR3022, and CT-P27) were 10 fold serially diluted from 2 to $2x10^{-7}$ µg/ml with serum-free media, OptiPRO SFM containing L-Glutamine (Gibco). SARS-CoV-2 (BetaCoV/Korea/KCDC03/2020) viruses (0.05 moi) were mixed with the diluted antibodies in the 96-well plate block (corning) for 2 h at 37ºC CO_2 incubator. In parallel, Raji and U937 cells ($2x10^4$/well) were prepared in U-bottom 96 well-plate. The inoculum from the plate block was added into VeroE6 cells, Raji cells and U937 cells and then incubated for 24 h at 37ºC CO_2 incubator. At 24 h post-infection, the cells were fixed with 80% acetone (Sigma). After washing, the cells were probed with SARS-CoV-2 anti-nucleocapsid antibody (Sino Biologicals, 1:2,000) and bound antibody was detected by horseradish peroxidase (HRP)-conjugated anti-mouse antibody (Southern Biotech, 1:4,000). Tetramethylbenzidine (TMB) was added and incubated for 5 min,

then stopped by H_2SO_4. Virus titres were assessed by optical density measured by spectrophotometer (Thermo Scientific) at 450 nm.

Animal experiments

All animal experiments were carried out according to the procedures approved by Chungbuk National University (CBNUA-1352-20-02), Agency for Defense Development (ADD-IACUC-20-12), Korea Research Institute of Bioscience and Biotechnology (KRIBB-AEC-20168) and complied with all relevant ethical regulations regarding animal research.

Ferret study

Groups of 14- to 18-month-old female ferrets (6/group) which are seronegative for SARS-CoV-1 and SARS-CoV-2, were inoculated intranasally and intratracheally with $10^{5.5}$ $TCID_{50}$ of NMC-nCoV02 (total 1 ml) under anaesthesia. Two doses, 3 and 30 mg/kg, of CT-P59 were administered intravenously 24 hr after virus inoculation in each group. Animals in the control group were given 30 mg/kg of human IgG isotype. Remdesivir (18 mg/kg) was administrated daily via oral gavage 24 h post-inoculation for 5 days. Body weights and temperatures were measured and nasal washes, saliva and rectal swab specimens were collected every other day. Three ferrets per group were euthanized at 3 and 7 dpi, and the nasal turbinates and lungs were subjected to measure tissue viral titres and examine lung histopathology. Viral titres in nasal washes and tissues were determined by $TCID_{50}$ assay in Vero cells, while the viral loads in saliva and rectal swab specimens were assessed using quantitative real-time PCR (qRT-PCR).

Golden Syrian hamster study

Sixty male golden Syrian hamsters (*n*=12/group) were challenged with 6.4×10^4 PFU/80 µl of SARS-CoV-2 via the intranasal route. Vehicle and 15, 30, 60 and 90 mg/kg CT-P59 were administered via an intraperitoneal route 24 hr after virus inoculation. At 2, 3, and 5 dpi four animals from each group were sacrificed for quantification of viral load in the lungs.

Rhesus monkey study

Eight rhesus monkeys (5 males, 3 females) were challenged with $2.6x10^6$ $TCID_{50}$ of SARS-CoV-2 via a combination of intranasal (0.5 ml), intratracheal (4 ml), ocular (0.25 ml/eye), and oral (5 ml) routes. CT-P59 (45 mg/kg (*n*=2) and 90 mg/kg (*n*=3)) was administered intravenously 24 hr after virus inoculation. Animals in the control group (*n*=3) were given an equal volume of vehicle. Viral load was measured by nasal, throat and rectal swabs daily until 6 dpi, and viral load in the lung was measured by necropsy at 6 dpi

Virus titration and quantitation

Virus titres in nasal washes and lungs ($TCID_{50}$) and in rectal swab (qRT-PCR) were determined. Briefly, viral titres for samples form the upper and lower airway were measured using Vero cells. All tissue

samples were diluted 10-fold (w/v) with sterile phosphate buffered solution (PBS, pH 7.4) and homogenized using a tissue homogenizer (Precellys Homogenizer, Bertin Instruments, France). After centrifugation of all swabs and homogenized tissue samples at 3,000 g for 10 min, the supernatants were filtered through 0.2 μm pore size syringe filter (Millipore, USA) and directly inoculated into Vero cells. The cells were incubated for 3 days at 37°C and then stained with crystal violet for cytopathic effect (CPE). The values of $TCID_{50}$/ml were determined using a Reed and Muench method.

In the ferret study, viral RNA was extracted using RNeasy kit (Qiagen) and cDNAs were reverse transcribed with a SARS-CoV-2 specific primer using QuantiTect Reverse Transcription (Qiagen). qRT-PCR reactions were performed using a SYBR Green Supermix (Bio-Rad). The viral RNA copy numbers were assessed by a CFX96 Touch Real-Time PCR Detection System (Bio-Rad) with a S gene based – SARS-CoV-2-specific primer and standard control[30]. In rhesus monkey study, total RNAs from the rectal swab sample were accessed by RT-qPCR. Viral RNA was extracted using a commercial viral RNA extraction kit (QIAamp Viral RNA Mini Kit, Qiagen). RT-qPCR was performed with a primer and probe set according to a previous report[43]. SARS-CoV-2 RNA standard samples were run in parallel for determination of virus copy number in all reactions.

Histology

Lung histology is evaluated as follows. Sections of the left caudal lung lobes were microscopically observed. Before collection, the lung lobes (with trachea intact) were insufflated with 10% neutral buffered formalin (NBF) and then submerged in 10% NBF for 2-3 days. Following fixation, the desired sections of lungs were embedded in paraffin, sectioned (5 μm), placed on glass slides, and stained with hematoxylin and eosin (H&E).

Human samples

The human samples were obtained according to the procedures approved by Seoul National University Hospital and complied with all relevant ethical regulations regarding human research. The blood was taken from a convalescent COVID-19 patient after she/he signed the informed consent form.

Reference For Methods

36 Kim, J. Y. *et al.* Viral Load Kinetics of SARS-CoV-2 Infection in First Two Patients in Korea. *J Korean Med Sci* **35**, e86, doi:10.3346/jkms.2020.35.e86 (2020).

37 Choi, J. H. *et al.* Characterization of a human monoclonal antibody generated from a B-cell specific for a prefusion-stabilized spike protein of Middle East respiratory syndrome coronavirus. *PLoS One* **15**, e0232757, doi:10.1371/journal.pone.0232757 (2020).

38 Kabsch, W. Xds. *Acta Crystallogr D Biol Crystallogr* **66**, 125-132, doi:10.1107/S0907444909047337 (2010).

39 McCoy, A. J. Solving structures of protein complexes by molecular replacement with Phaser. *Acta Crystallogr D Biol Crystallogr* **63**, 32-41, doi:10.1107/S0907444906045975 (2007).

40 Emsley, P. & Cowtan, K. Coot: model-building tools for molecular graphics. *Acta Crystallogr D Biol Crystallogr* **60**, 2126-2132, doi:10.1107/S0907444904019158 (2004).

41 Adams, P. D. *et al.* PHENIX: a comprehensive Python-based system for macromolecular structure solution. *Acta Crystallogr D Biol Crystallogr* **66**, 213-221, doi:10.1107/S0907444909052925 (2010).

42 Janson, G., Zhang, C., Prado, M. G. & Paiardini, A. PyMod 2.0: improvements in protein sequence-structure analysis and homology modeling within PyMOL. *Bioinformatics* **33**, 444-446, doi:10.1093/bioinformatics/btw638 (2017).

43 Chu, D. K. W. *et al.* Molecular Diagnosis of a Novel Coronavirus (2019-nCoV) Causing an Outbreak of Pneumonia. *Clin Chem* **66**, 549-555, doi:10.1093/clinchem/hvaa029 (2020).

Declarations

Data and code availability

The atomic coordinates and structure factor files for the CT-P59 Fab/SARS-CoV-2 RBD complex have been deposited in the Protein Data Bank (PDB) under accession number 7CM4. The data that support the findings of this study are available from the corresponding authors upon reasonable request.

Acknowledgements

This study was supported by a Korea National Institute of Health fund (2020-ER5311-00, 2020-ER5323-00, 2019-NI-077-01, 2019-NG-044-01), grants (011555-012664201) from the Agency for Defense Development, grants (PRM1752011) from the Ministry of Science and ICT, and partially supported by the Korea Research Institute of Bioscience and Biotechnology (KRIBB) Research Initiative Program (KGM9942011), Republic of Korea.

Author contributions

C.K. and J.M.S. initiated and managed to identify CT-P59 from convalescent patient with COVID-19. Y.J.A. narrowed down RBD binding candidates by ELISA with help of C.K. and J.M.S. M.S.K. and G.S.P. carried out cloning and expression of CT-P59 and recombinant RBD protein. M.K. and H.N. conducted BLI with Octet. J.S.P. and M.S.L conducted SPR. E.Y.S. and J.N.L. carried out purification of antibody and antigen. P.K. contributed to mode of action study with D.K.R. who performed *in vitro* ADE. J.I.K. and D.S. managed and analyzed the animal experiments. K.S.K. and S.Y.L. coordinated overall CT-P59 project. J.Y.L., H.L., J.S.Y., K.C.K., S.S.K., H.M.W. and J.W.K. isolated human PBMC from whole blood and performed *in vitro* PRNT with the help of C.K., J.M.S. and M.K, against wild and D614G variant with the help of M.S.P. Y.K.C.,

Y.I.K., K.M.Y., S.M.K., E.H.K. and S.J.P. performed animal experiments with ferrets. S.T.J., C.H.Y., Y.S. and S.H.G. performed animal experiments with golden Syrian hamsters with the help of J.Y.L., J.W.K., H.M.W., J.S.Y. and K.C.K. who performed *in vitro* $TCID_{50}$. H.O., B.S.K., J.J.H. and C.M.R. performed animal experiments with rhesus monkeys. W.B.P. and M.D.O. recruited patients recovered from COVID-19. Y.G.K., J.H.J. J.L. and J.S.B. carried out crystallization, diffraction data collection, structure determination and analysis of CT-P59 and RBD complex. C.K., D.K.R., J.L., J.I.K., Y.K.C. and S.Y.L. analyzed the data and wrote the manuscript.

Competing interest

Patents have been filed for CT-P59. C.K., D.K.R., J.L., J.M.S., M.K., J.I.K., P.K., J.S.B., E.Y.S., M.S.L., M.S.K., H.N., G.S.P., J.S.P., D.S., Y.A., J.N.L., K.S.K. and S.Y.L. are employees of Celltrion, Inc. This work was funded by Celltrion, Inc. and several grants listed in Acknowledgements.

Additional information

Correspondence and requests for materials should be addressed to S.Y.L and Y.K.C.

Figures

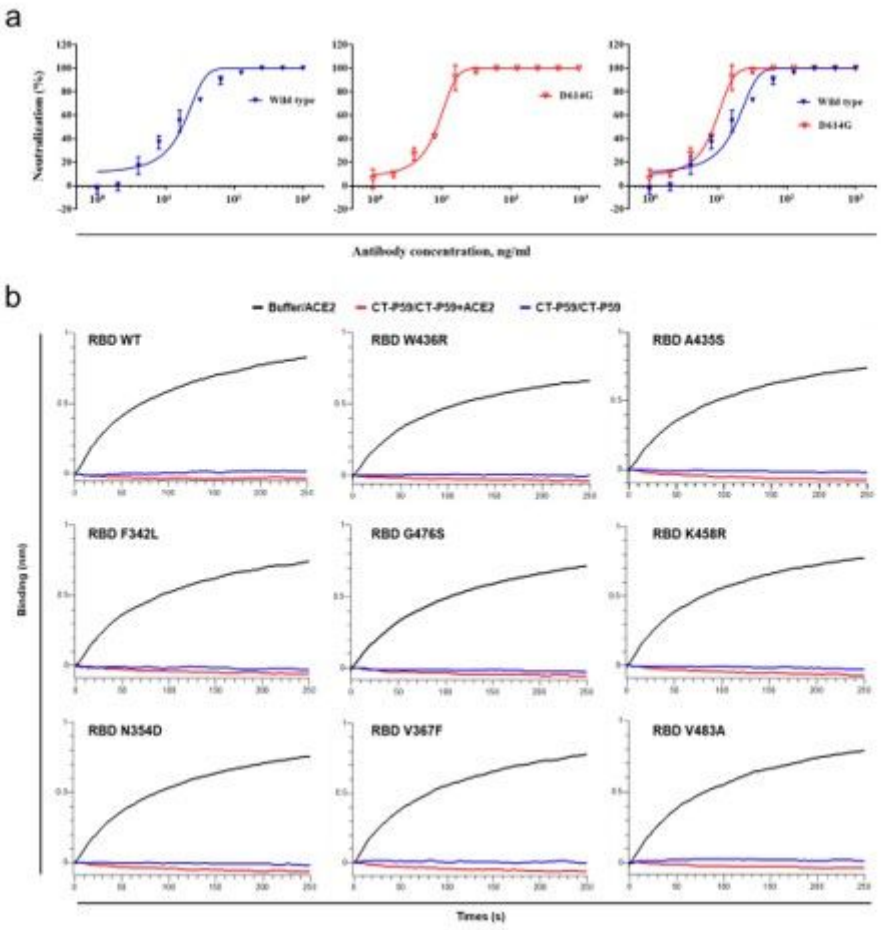

Figure 1

| CT-P59 can effectively neutralize SARS-CoV-2 in vitro by blocking RBD-ACE2 binding. a, Serial 2-fold-diluted CT-P59 were incubated with SARS-CoV-2 live viruses; wild type (blue) and D614G (red). The mixture was added to VeroE6 cells. After 2 to 3 days of incubation, the neutralization activity was evaluated by counting plaques. Two independent experiments were performed in duplicate. b, SARS-CoV-2 RBD immobilized on biosensor was saturated with CT-P59. Then, CT-P59 was flowed over the biosensor surface in the presence or absence of ACE2 receptor. As a positive control, buffer was loaded onto SARS-CoV-2 RBD immobilized biosensor, and ACE2 was flowed over the biosensor surface.

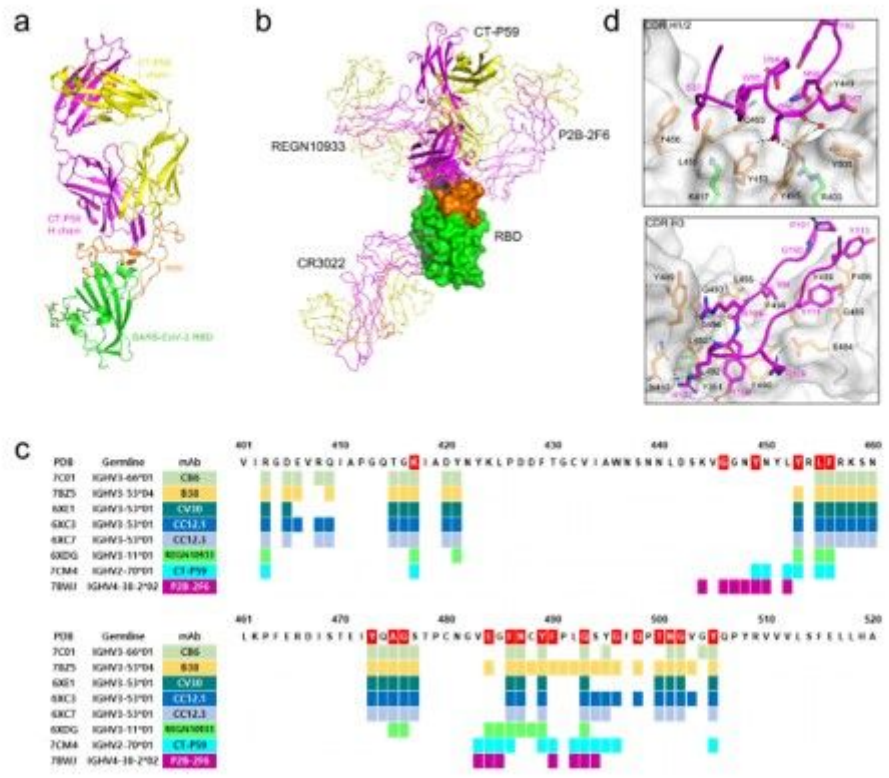

Figure 2

The structure of CT-P59 Fab in complex with SARS-CoV-2 RBD. a, The overall structure of the CT-P59 Fab/SARS-CoV-2 RBD complex. The RBD domain is green for the core subdomain and orange for RBM. The heavy and light chains of CT-P59 are magenta and yellow, respectively. b, Superposition of the neutralizing antibodies in complex with RBD. RBD is shown as a surface model. CT-P59 is shown as a cartoon, and the other antibodies (CR3022: PDB 6XC3, PB2-2F6: PDB 7BWJ, REGN10933: PDB 6XDG) are shown as a ribbon model. The heavy and light chains of Fab are magenta and yellow, respectively. c, Assignment of the epitope residues for RBD-targeting neutralizing antibodies with a distance cut-off of 4.5 Å. RBD residues interacting with ACE2 are highlighted in red. d, The detailed interactions between the RBD and CDR loops of CT-P59. The interfaces between RBD and CDR H1/2 or H3 are shown in the top and bottom panels, respectively. The RBD domain is shown as a surface model with semi-transparent representation. The CDR loops and interacting residues on the interfaces are shown in ribbons and sticks, respectively. The residues are coloured as in a. Dashed lines indicate hydrogen bonds. Water molecules are shown as red spheres.

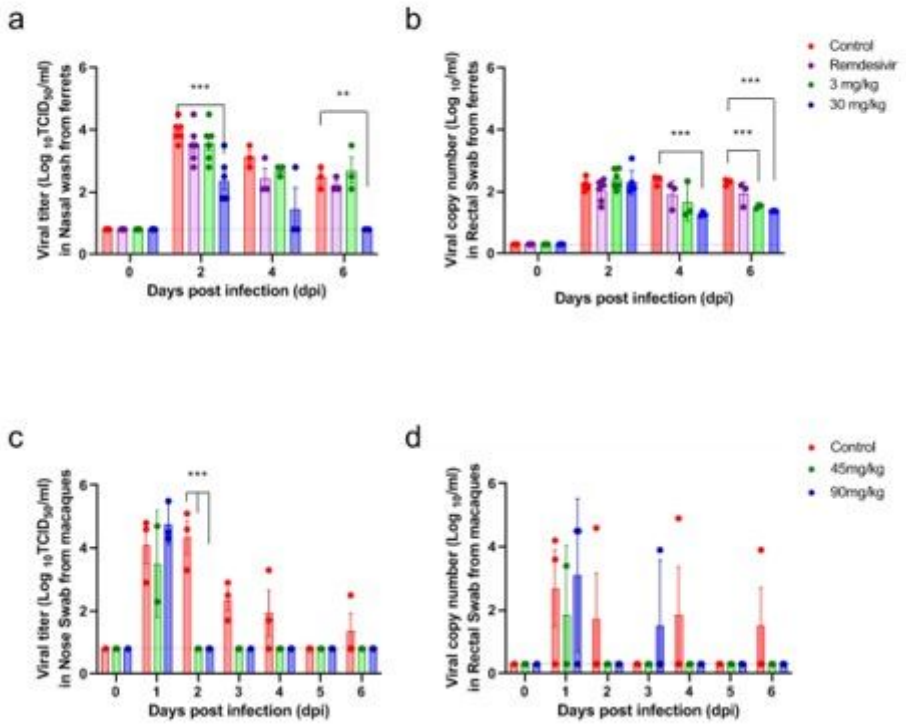

Figure 3

| In vivo efficacy of CT-P59 in animal models. Female ferrets (n=6/group), and rhesus monkeys (three control; two 45 mg/kg; three 90 mg/kg) were challenged with 105.5 TCID50/ml and 106.4 TCID50 of SARS-CoV-2, respectively. Control (ferrets: 30 mg/kg of human IgG isotype and rhesus monkeys: vehicle) and CT-P59 (ferrets: 3, and 30 mg/kg, rhesus monkeys: 45, and 90 mg/kg) were administered intravenously after 24 hours of virus inoculation, respectively. To compare the efficacy of CT-P59, Remdesivir (18 mg/kg per ferret) was administered daily via oral gavage after 24 hours of virus inoculation in ferrets for 5 days. To detect the viral load, nasal wash/swab and rectal swabs specimens were collected at 2, 4, and 6 dpi. Virus titres (TCID50) were measured in nasal wash specimens from each group of (a) ferrets and, (c) rhesus monkeys. The number of viral RNA copies was measured in rectal swabs from each group of (b) ferrets and, (d) rhesus monkeys using qRT-PCR. Viral titres and RNA copy numbers are shown as means ± SEM from four animals and titres below the limit of detection are shown as 0.8 log10TCID50/ml or 0.3 log10 viral RNA copies/ml (dashed lines). * indicates $P < 0.01$, ** indicates $P < 0.001$, and *** indicates $P < 0.0001$ between the control and each group as determined by two-way ANOVA and subsequent Dunnett's test.

Supplementary Files

This is a list of supplementary files associated with this preprint. Click to download.

- SupplementaryTable14Aug2020.docx

- ExtendedData14Aug2020.docx